Forest Ecology and Management 406 (2017) 83–94

Contents lists available at ScienceDirect

Forest Ecology and Management

journal homepage: www.elsevier.com/locate/foreco

Comparison of lidar- and allometry-derived canopy height models in an eastern deciduous forest

Franklin B. Sullivan[a,*], Mark J. Ducey[b], David A. Orwig[c], Bruce Cook[d], Michael W. Palace[a,e]

[a] Earth System Research Center, Institute of Earth, Oceans, and Space, University of New Hampshire, Durham, NH, United States
[b] University of New Hampshire, Department of Natural Resources and the Environment, Durham, NH, United States
[c] Harvard Forest, Harvard University, Petersham, MA, United States
[d] NASA Goddard Space Flight Center, Greenbelt, MD, United States
[e] University of New Hampshire, Department of Earth Sciences, Durham, NH, United States

ARTICLE INFO

Keywords:
Crown allometry
Tree height
Canopy height model
Mixed effects modeling
Fast Fourier transform

ABSTRACT

Tree crown geometry and height, especially when coupled with remotely sensed data, can aid in the characterization of tree and forest structure. In this study, we develop mixed-effects model allometric equations for tree height, crown radius, and crown depth using data collected on 374 trees across 14 species within the extent of the joint Center for Tropical Forest Science (CTFS) and Smithsonian Institute's Forest Global Earth Observatory (ForestGEO) MegaPlot on Prospect Hill at Harvard Forest, Massachusetts. We applied allometry to a census of the 35-ha plot on Prospect Hill to evaluate tree height and crown radius estimates using a lidar canopy height model. We found significant relationships using stem diameter-at-breast-height (*DBH*) and species to estimate tree height (ρr^2 = 0.70, RMSE = 2.96 m), crown depth (ρr^2 = 0.35, RMSE = 3.24 m) and crown radius (ρr^2 = 0.43, RMSE = 1.22 m). Using Fast Fourier Transforms (FFTs), we compared the power spectra of a lidar canopy height model to five synthetic canopy height models derived from allometric estimates of height and crown radius. The FFTs showed good agreement between lidar and synthetic canopy height models (CHMs) at spatial wavelengths longer than 64 m, or about the distance across 3–4 dominant tree crowns, and poorer agreement at shorter spatial wavelengths, which we attribute to the simple crown shape applied to modeled crowns and a lack of crown overlap in the synthetic CHMs compared to the lidar CHM. At the tree level, some species exhibited tight links between lidar-measured height and estimated tree height (e.g., *Quercus rubra*, *Quercus velutina*, *Pinus strobus*), suggesting height allometry provided reasonable estimates of tree height for some species despite a negative bias in the synthetic canopy height models relative to the lidar canopy height model.

1. Introduction

The structural status of forests is driven by processes of carbon uptake, disturbance regimes, and their historical trajectories (Frolking et al., 2009, Espirito-Santo et al., 2014), and is influenced by complex interrelationships of architectural components of trees. Understanding relationships among different characteristics of tree and forest structure (e.g., stem diameter, canopy height, crown geometry, species assemblages, aboveground biomass) is critical to assessing and extrapolating field measurements to inaccessible sites using remote sensing data (e.g., Spies, 1998; Xie et al., 2008; Frolking et al., 2009; Saatchi et al., 2011; Homolova et al., 2013, Meyer et al., 2013; Mauya et al., 2015; Palace et al., 2015). To best utilize the advances in remote sensing technologies for forest demography and biomass research, it is necessary that site-specific field-data driven allometric models are developed and tested (Hunter et al., 2013). In particular, estimation of stand biomass using remote sensing tools, e.g. light detection and ranging (lidar), could greatly benefit from tree-level allometry, such as height and crown geometry (Dalponte and Coomes, 2016), as well as automated tree crown detection tools (Palace et al., 2008; Duncanson et al., 2015; Ferraz et al., 2016). If such characteristics of trees can be statistically linked to bole biomass predictors, such as stem diameter at breast height (*DBH*), stand biomass estimation can theoretically be scale-invariant using commonly used allometric equations to estimate biomass at the tree-level (Zhao et al., 2009).

Many studies have used remote sensing data, specifically lidar, to characterize and monitor forest structure. Approaches to characterizing biomass across large areas at large spatial scales (ranging from hectares

* Corresponding author at: 462 Morse Hall ESRC, 8 College Road, Durham, NH 03824, United States.
E-mail address: fsulliva@gmail.com (F.B. Sullivan).

http://dx.doi.org/10.1016/j.foreco.2017.10.005
Received 17 July 2017; Received in revised form 2 October 2017; Accepted 3 October 2017

to square kilometers) using relationships developed between field data and lidar metrics are common (Dubayah et al., 2010; Ni-Meister et al., 2010; Saatchi et al., 2011; Yao et al., 2011; Asner et al., 2012; Palace et al., 2015; Manuri et al., 2017). Typically, biomass allometry for estimation using lidar data use a range of modeling approaches to relate field-estimated biomass (i.e. calculated by *DBH* allometry) to lidar-derived metrics like mean canopy height at the plot level, lidar maximum height, energy or return percentiles, and more complex metrics like entropy (Lefsky et al., 1999; Dubayah et al., 2010; Saatchi et al., 2011; Treuhaft et al., 2014; Sullivan et al., 2014; Palace et al., 2015; Palace et al., 2016). Recent applications have used lidar for mapping logging roads and skid trails in order to estimate the carbon impact of logging operations (e.g. Anderson et al., 2014; Ellis et al., 2016). These approaches to biomass estimation and carbon impacts of logging, however, have mostly been successful at scales ranging from hectares to kilometers, and estimates are generally mapped across landscapes and regions, as opposed to the individual tree-level, which theoretically could be aggregated for plot and regional estimates of biomass (van Leeuwen and Nieuwenhuis, 2010).

For tree- and plot-level field based biomass estimates, allometric equations have been developed predominantly using *DBH*, though some have been established with height modifiers (e.g. Chave et al., 2005). The allometric uncertainty associated with *DBH*-only models typically impacts the first significant digit of ensuing estimates, especially when models are applied outside the population within which they were developed (Kershaw et al., 2016), and as it represents a form of bias it does not vanish with increasing sample size. Hunter et al. (2013) demonstrated, however, that plot-level field biomass estimates that also incorporate height are subject to 5–6% error due to imprecise tree height measurements in dense forests. To that end, site-specific height allometry or accurate height measurements using lidar to retrieve tree-level heights could serve to reduce measurement error and improve biomass estimation uncertainty. Furthermore, *DBH*-height allometric equations have been developed for individual sites and globally (e.g. Feldspauch et al., 2011), which when used out-of-population or (in the case of regional or global equations) at specific sites can result in even greater uncertainty in biomass estimates (Hunter et al., 2013). For a thorough treatment of *DBH*, height, and tree volume or biomass allometry, see Kershaw et al. (2016, ch. 6).

It is possible that remote sensing estimates of biomass could stand to be improved further by including crown size variables in models. Indeed, Goodman et al. (2014) showed significant improvement in aboveground biomass estimates when accounting for tree crown radius. Other studies have also shown that tree crown variability is useful for estimating biomass. Jucker et al. (2017) developed a global database of stem diameter, height, and crown diameter, and go on to show that crown diameter and tree height can be used to estimate both stem diameter and aboveground biomass of individual trees. Ferraz et al. (2016) applied crown detection techniques to estimate tree and crown shape characteristics, then developed biomass equations which they assessed at multiple scales. Approaches to remote biomass estimation using crown geometry characteristics will prove most useful when combined with rapid and accurate tree crown delineation (Swetnam and Falk, 2014; Ferraz et al., 2016), but even given success, there are challenges to linking crown geometry and biomass at the tree-level caused by crown plasticity.

Because vertical and horizontal accuracies of commercial airborne lidar systems are generally around ± 15 cm and ± 50 cm, it is a valuable tool that can be used for assessing field-based allometric models. At tropical forest sites and some low complexity temperate sites, crown geometry has been assessed and compared from both field-based and remote sensing measurements (e.g. Asner et al., 2002; Broadbent et al., 2008; Palace et al., 2008). Although it would be useful for directly assessing tree-level height and crown geometry allometry, efforts to compare lidar remote sensing measurements to field-based estimates are relatively uncommon in mixed deciduous temperate forests. Here, we examine the potential to assess height and crown allometry using lidar data at Harvard Forest, a temperate forest site in Petersham, Massachusetts. The motivation for this study was to demonstrate the development of mixed effects allometric models for tree height and crown geometry, which we apply to census data of a 35-ha plot to develop a simple canopy height model (CHM). Using multiple error correction approaches for the allometry, we estimate the power spectra of their 2-dimensional Fast Fourier Transforms which we use to compare CHMs at the site level and at finer spatial scales. To assess allometric equations for tree height, we compared the synthetic allometric canopy height models to the lidar canopy height model at the species-level. Lastly, we leverage our comparison between lidar and allometric CHMs to evaluate allometric relationships in the context of plant functional traits, crown plasticity and structural variation, and tree form models.

2. Methods

2.1. Field census

Between June 2010 and March 2014, a census of a 35-ha plot on the Prospect Hill Tract in Harvard Forest, Massachusetts was conducted in a joint effort by the Center for Tropical Forest Science (CTFS) and the Smithsonian Institute's Forest Global Earth Observatory (ForetGEO) as part of the MegaPlot network (Anderson-Teixeira et al., 2015). Within the extent of the plot (Fig. 1), all woody stems ≥1 cm stem *DBH* were identified by species and tagged, and stem diameter was measured using a diameter tape. The census was completed by numerous field technicians, with quality control and quality assurance completed according to CTFS ForestGEO protocol and methodology (http://www.ctfs.si.edu/). In total, approximately 116,000 woody stems were recorded during the census with 51 unique species identified (Orwig et al., 2015).

2.2. Field-based measurements of canopy geometry

In September and October 2013, variable radius plot sampling (Bitterlich, 1984) was completed within the extent of the ForestGEO plot. Thirty-nine randomly selected plots were located approximately using a handheld Garmin GPSmap 76CSx handheld GPS unit (error ± approx. 5 m). Actual plot centers were recalculated post hoc by calculating the centroid of the $UTM_{x,y}$ locations of tagged trees in the Prospect Hill Tract plot space relative to the x,y locations of the same trees in the local coordinates of the variable radius plot. At each plot, a 4.59 m^2/ha basal area factor prism was used to sample trees 5 cm and greater *DBH*; the sample trees thus represent a size-weighted sample of the full population of the trees over 5 cm *DBH* on the tract (Kershaw et al., 2016, ch. 9). At each sampled tree, we recorded species and tag number (except where they had fallen off or not been measured for census yet), as well as measured the distance and bearing from plot center, *DBH*, tree height, crown base height, and crown radius toward and away from plot center. This pair of crown radii can be used to estimate crown area without bias, irrespective of crown shape (Gregoire and Valentine, 1995). Crown radii and tree height measurements were made using a laser range finder with a viewfinder and integrated tilt sensor (DISTO D5, Leica Geosystems). Crown radii were measured by using the viewfinder to determine when the observer was under the dripline of the tree crown toward and away from plot center, and by measuring the distance to the stem using a laser range finder which was subsequently adjusted for the distance between stem face and stem center.

2.3. Allometry and canopy height models

2.3.1. Mixed effects modeling

Allometric equations were developed in R (version 3.0.1) using a

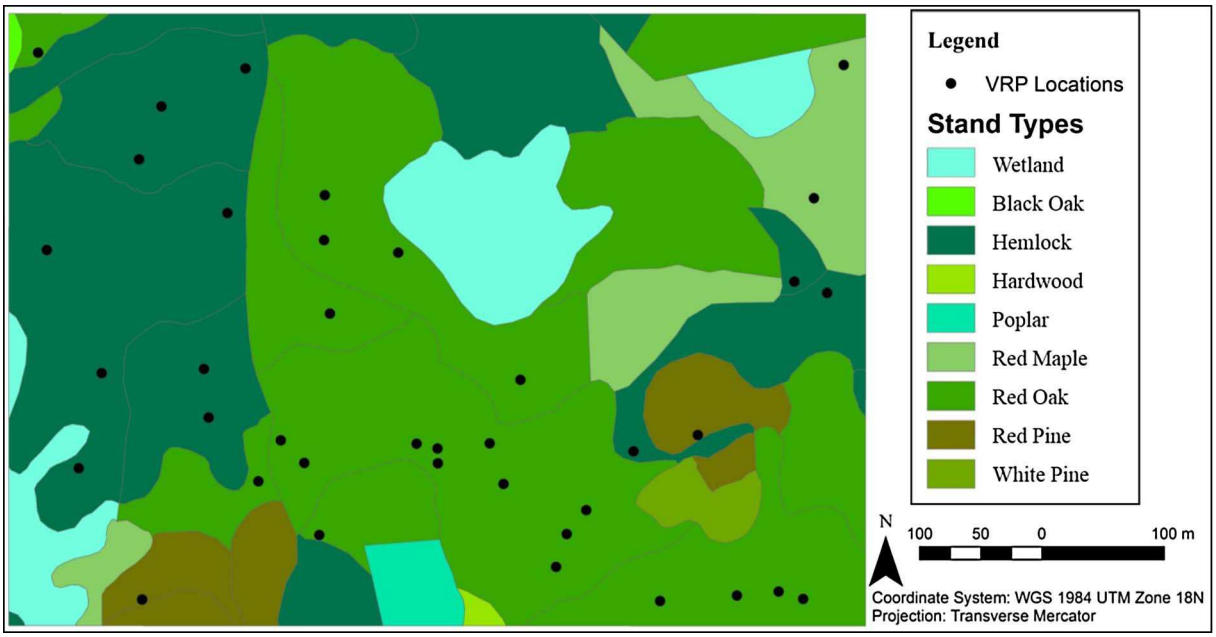

Fig. 1. A 1993 stand map within the extent of the Prospect Hill census plot showing the primary species within each stand except for within wetland areas with random plot locations marked as black dots.

mixed effects modeling approach in the lme4 package. In this study, we used mixed effects models in order to account for the random effects of plot (i.e. unmeasured site quality and past competition effects) and species to assess the extent to which variation in the data were linked to either or both, and to ensure models were efficiently fit. For all models *DBH* was used as the fixed effect. For modeling tree height, *DBH* was inverse-transformed and height was log-transformed, i.e.

$$\ln(H_I) = \beta_0 + \gamma_{0,s(i)} + \delta_{0,p(i)} + (\beta_l + \gamma_{l,s(i)} + \delta_{l,p(i)})/DBH_i + \sigma_i$$

where β_0 and β_1 are fixed effect parameters, $\gamma_{0,s(i)}$ and $\gamma_{1,s(i)}$ are random effects associated with the species of tree i, $\delta_{0,p(i)}$ and $\delta_{1,p(i)}$ are random effects associated with the plot on which tree i occurs, and σ_i is the residual. This model is a mixed-effects version of the Schumacher and Hall (1933) regression, which is among the most widely used models for height-diameter relationships in forestry. For crown radius and crown depth, we used untransformed linear models with the same base structure, i.e.,

$$y_i = \beta_0 + \gamma_{0,s(i)} + \delta_{0,p(i)} + (\beta_l + \gamma_{l,s(i)} + \delta_{l,p(i)})*DBH_i + \sigma_i$$

where y_i is crown radius or crown depth as appropriate. Final predictive models were determined using Akaike Information Criterion (AIC) to compare model strength. We also calculated a pseudo coefficient of determination (ρr^2), which we used to assess the added predictive power of the plot and species effects, as:

$$1-\frac{\sum (M-ME_{est})^2}{\sum \left(M-\frac{1}{n}\sum M\right)^2}$$

where the numerator is the sum of squared residuals, and the denominator is the sum of squares; M is the measured value of the variable and ME_{est} is the mixed effects model estimate.

2.3.2. Transformation bias correction and error imputation

For two of the modeled variables, the naive application of a regression model would entail bias. In the case of tree height, because tree height is log-transformed in the regression a well-studied form of bias occurs (e.g. Finney, 1941; Zar, 1968; Baskerville, 1972): the regression prediction is the mean of log height, rather than height, conditional on the predictor variables, so a systematic underprediction occurs. This type of error is particularly well understood in allometric modeling of biomass, where log-transformation is commonly applied both to linearize the relationship and to eliminate heteroscedasticity (Kershaw et al., 2016, ch. 5 and 6). As an alternative to linear regression using log-transformed height, we might have applied nonlinear mixed-effects modeling to predict height directly, while simultaneously modeling heteroscedasticity through maximum likelihood; however, such models are not guaranteed to be bias-free and can present computational challenges such as lack of convergence (e.g. Fast et al., 2011). Dealing with the bias in a log-transformed regression thus represents an attractive option. In the case of crown radius, there is appreciable error in the field measurement of crown area; although crown area is estimated without bias for individual trees, crown radius is a nonlinear function of crown area so its estimate is attended by a slight bias. We applied four error accounting strategies, from each of which we developed a synthetic CHM derived from the census data to compare to the lidar CHM. In total, we calculated five estimates of combinations of tree height and crown geometry: 1. uncorrected, 2. height retransformation bias correction, 3. height errors imputed, 4. crown radius errors imputed, 5. height and crown radius errors imputed. We calculated retransformation bias corrected estimates of tree height, H_{bc}, as:

$$H_{bc} = H\exp\sigma^2/2$$

where H is the uncorrected height estimate and σ^2 is the variance of the residuals (computed in the log-transformed space). This approach is used to account for the disproportionate underestimation of the heights of tall trees resulting from the log transformation in allometric models (Baskerville, 1972; Czaplewski and Bruce, 1990). As an alternative, we imputed errors into height and crown geometry estimates. To do this, for each tree we added residual errors of height and crown geometry for a randomly selected measured tree to the height and crown geometry estimates for each tree. These approaches combined with a comparison of CHMs were intended to inform this analysis of any bias and errors in allometric models, and specifically whether systematic over- or underestimates associated with either the tree height or crown radius models had an appreciable impact on the resulting synthetic CHMs.

2.3.3. Canopy height model calculation

Coincident lidar data was collected by the Goddard Lidar, Hyperspectral, and Thermal (G-LiHT) sensor package (Cook et al.,

2013) in June 2012 over the Prospect Hill Tract. The lidar 1 m spatial resolution CHM product was downloaded on November 10, 2014 (gliht.gsfc.nasa.gov/downloads). It was derived by calculating the difference between a digital surface model and digital terrain model and clipped to the extents of the Prospect Hill Tract census (501 × 701 pixels). In addition, we generated synthetic CHMs by applying the allometric estimates of tree height and crown shape from the ForestGEO plot census using each of the five error accounting strategies used. As described in the previous section, allometric equations were applied to the census data set using the estimated intercept and slope of the fixed effect of *DBH* and the random effect of species to estimate crown depth, crown width, and tree height. For species that were not sampled, the mean allometry (i.e. only the fixed effect) was applied to estimated tree height and crown geometry. From estimated crown geometry, synthetic CHMs were developed using the surface of an ellipsoid for each tree on the same grid as the lidar CHM. Canopy surfaces were assumed to have an ellipsoidal shape in the vertical dimension, and because crown width was measured along only one axis, trees were assumed to be circular in the horizontal dimension. For each tree, the footprint of the tree crown was calculated using the estimated crown radius, r, and the x,y coordinates of the stem, assuming that the coordinate pair also represented the location of the center of the tree crown, x_c,y_c. Within each crown footprint, the height, z, at each pixel center was calculated as:

$$z = \sqrt{\left(\left(1-\left(\frac{x_c^2}{r^2}\right)-\left(\frac{y_c^2}{r^2}\right)\right)*\left(H-\frac{D}{2}\right)^2\right)} + \left(H-\frac{D}{2}\right)$$

where H is the estimated total height of the tree and D is the estimated crown depth. In instances where multiple trees overlapped with an individual pixel, the maximum height assigned to the pixel was used.

2.4. Statistical analysis

2.4.1. Tree- and species-level canopy height model comparison

We compared the lidar and all allometric CHMs at both the individual tree and species scales. To accomplish this, we identified the stem ID of the crown represented in each CHM pixel. During generation of synthetic CHMs, as heights were calculated and assigned to each pixel the stem ID of the tree canopy surface calculated was assigned to the same pixel in a second grid, the stem ID map. We calculated a total of five stem ID maps; one for each of the four error accounting strategies, and one for the uncorrected CHM. Using the set of unique identifiers in the stem ID maps, we calculated mean and maximum heights for all individual stems from each of the synthetic CHMs and for the same set of stem ID footprints for the lidar CHM.

At the tree level, we compared lidar stem heights to all synthetic CHM stem heights by a correlation analysis in R (v. 3.0.1). At the species level, we calculated the mean and standard deviation of mean and maximum canopy heights of each individual tree of a species and compared lidar and synthetic heights grouped by species using paired Student's *t*-tests in R. For these correlation analyses, individual trees identified using the stem ID maps were used as the observations.

2.4.2. Whole-image canopy height model comparison

In order to assess overall similarity between CHMs and specific scales at which synthetic CHMs and the lidar CHM were in agreement with each other, we compared the power spectra of their Fast Fourier Transforms (FFT). For each image, we calculated the FFT in Python (v. 2.7) using the numerical computation package NumPy (v. 1.11.3, van der Walt et al., 2011). Prior to calculating FFTs, in order to minimize artefacts due to the edge of the original CHM, a larger image was created (1503 × 2103 pixels). For each CHM, the larger image had the same properties of the original image by padding by its mirror on the four x and y axes and the four diagonals. Recovery of power spectra from FFTs implies an assumption that the image is periodic, wrapping seamlessly around each edge. An actual CHM is not periodic, because the heights on the east edge do not match those on the west, and those on the north edge do not match those on the south. Reproducing this sharp discontinuity would require substantial power at short wavelengths, and the resulting spectral leakage would mask the actual power spectrum at those wavelengths. Appropriate padding eliminates the sharp edge and the resulting artefact in the power spectrum. Using the x- and y-component frequencies sampled for a 1503 × 2103 pixel image, we calculated the total frequency for each FFT pixel as:

$$F = \sqrt{x^2 + y^2}$$

and the spatial wavelength, ω, for each FFT pixel follows as:

$$\omega = 1/F$$

which we rounded to the nearest 1 meter, the spatial resolution of the CHM images. In other studies, images have been cropped to square prior to calculating the FFT in order to estimate an azimuthally averaged power spectrum of a 2-dimensional FFT (e.g. Sinclair and Pegram, 2005). Here, we proceeded to estimate the mean 1-dimensional power spectra of the 2-dimensional FFTs as the mean FFT magnitude at each rounded sampled $\omega \leq 862$ m. As a way to assess agreement at different spatial scales, we compared mean power of the lidar CHM to each of the synthetic allometric CHMs using two-sided *t*-tests at each sampled ω.

3. Results

3.1. Height and crown geometry allometry

Using the variable radius plot sampling approach, we collected stem measurements for 374 individual trees across 14 species, 342 of which were live trees, with sampled species representing 97.1% of the total basal area in the 35-ha tract (Table 1). Significant positive relationships resulted from modeling crown radius, crown depth, and tree height using *DBH* (Fig. 2). By accounting for species in models, we observed marked improvement in both ρr^2 and RMSE for tree height and crown geometry measures. We observed no significant improvement in models by including the random effect of plot for tree height, but for crown radius ρr^2 improved from 0.434 to 0.618, with a 0.22 m difference in RMSE compared to using the mean plot effect, and for crown depth, accounting for plot resulted in a ρr^2 of 0.471 and RMSE of 2.93 m compared to 0.35 and 2.96 m, respectively, when applying the mean plot effect (see Table 2). The fixed effect (DBH) coefficients and the random effect (species) coefficients for 14 species are reported in Table 3. Height and crown radius, and their respective species effects were also significant predictors of *DBH* with the mean plot effect, which contributed significantly to the model (mean plot effect: $\rho r^2 = 0.60$, RMSE = 8.3 cm, CV (RMSE) = 24.5%; varied plot effect: $\rho r^2 = 0.64$, RMSE = 7.9 cm, CV (RMSE) = 23.3%).

Table 1
Species sampled for allometric equation development and their sample sizes, DBH distribution, and percent of basal area represented by each in the Prospect Hill Tract census.

Species	N	DBH mean	DBH range	Census BA%
Acer rubrum	56	23.75	4.6–45.5	17.1
Betula alleghaniensis	8	22.31	11.3–30.4	2.6
Betula lenta	6	22.08	6.7–36.5	1.3
Betula papyrifera	2	24.75	23–26.5	1.3
Fagus grandifolia	2	24.35	20–28.7	1.5
Fraxinus americana	3	32.9	19.7–41.5	0.3
Kalmia latifolia	1	4.5	4.5	0.2
Picea abies	14	25.93	12.5–49.5	2
Picea rubens	1	29.5	29.5	0.2
Pinus resinosa	28	35.53	22.4–43.4	4.5
Pinus strobus	42	46.21	18–71.1	11.1
Quercus rubra	85	38.95	15–65.8	21.2
Quercus velutina	6	33.95	22.3–46.2	1.2
Tsuga canadensis	88	33.14	9–68.6	32.6
Total	342	33.85	4.5–71.1	97.1

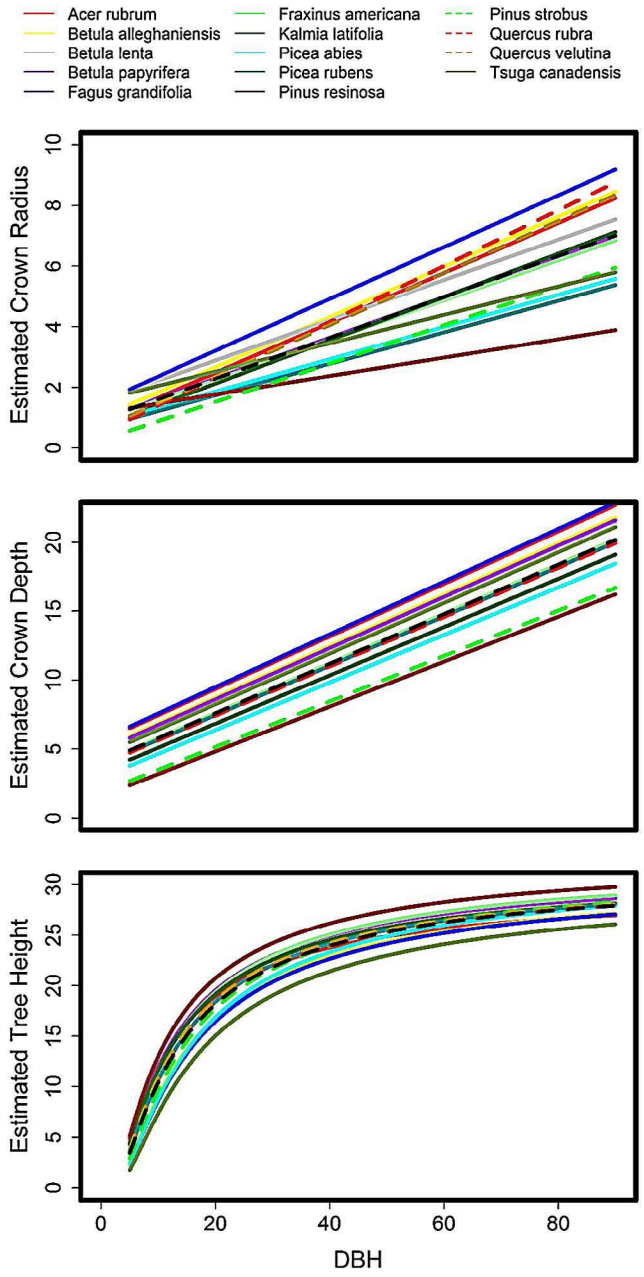

Fig. 2. Positive relationships with varying slope and intercept for 14 unique species and the mean relationship for crown radius, depth, and tree height at Harvard Forest.

3.2. Tree- and species-level canopy height model comparison

The CHMs each consisted of a total of 351,201 pixels. Of these, for the uncorrected, bias corrected, and height error imputation CHMs, 84.6% of the pixels contained height data for species that were sampled in the variable radius plots. For CHMs using crown radius error imputation estimates, 88.9% of the pixels contained height data for species sampled in the variable radius plots. The within crown pixels were distributed across an average of 25,112 individual exposed tree crowns, with a mean of 12.43 pixels per tree. Mean individual-tree canopy height, calculated by averaging the height of all pixels within each of the tree crown extents, varied for the lidar and synthetic CHMs across the five error accounting approaches (Table 4a). Although the different error accounting approaches do not alter the original lidar CHM itself, they do impact the assignment of individual pixels in the CHM to individual trees; thus, changing the treatment of variability within the allometry impacts the individual-tree estimates of canopy height. For all stems, regardless of species, lidar-estimated canopy heights and synthetic CHM canopy heights were moderately to strongly correlated, regardless of the correction applied, but with some apparent underestimation of allometry heights when compared to the lidar CHM (Fig. 3, Table 4b).

Within species sampled in the field, we observed moderate to strong correlations between lidar and synthetic CHM estimated canopy heights (Table 4b). Accounting for transformation bias and error imputation did not significantly improve the correlation for all species, but did marginally improve the agreement between mean and maximum species heights based on height comparisons (Tables 5 and 6). Using *t*-tests, we observed significant differences in mean individual-tree canopy height as estimated by lidar and synthetic CHMs for most species. Although differences remained statistically significant for most species following bias correction or error imputation, the difference between lidar and synthetic CHM mean and maximum canopy heights within species were generally reduced (Tables 5 and 6). Differences in means were reduced

Table 3
Allometric equations of crown radius, crown depth, and tree height. If a species is not in the table, the species effect is set to zero for prediction.

	Crown radius		Crown depth		Total height	
	Intercept	Slope	Intercept	Slope	Intercept	Slope
Fixed effects (β_0,β_1)	0.937	0.067	3.997	0.180	3.452	−11.059
Species effects (γ_0,γ_1)						
Acer rubrum	−0.101	0.015	1.561	0.011	−0.057	2.003
Betula alleghaniensis	0.075	0.015	1.009	0.007	−0.014	−1.264
Betula lenta	0.621	−0.001	0.790	0.005	−0.005	1.277
Betula papyrifera	0.015	0.000	0.890	0.006	0.012	1.213
Fagus grandifolia	0.571	0.018	1.676	0.012	−0.012	−1.718
Fraxinus americana	−0.012	−0.002	0.027	0.000	0.027	0.722
Kalmia latifolia	−0.237	0.004	−0.657	−0.005	−0.005	1.168
Picea abies	−0.138	−0.014	−1.061	−0.007	0.021	−1.896
Picea rubens	−0.237	−0.015	−0.107	−0.001	0.003	0.212
Pinus resinosa	0.228	−0.037	−2.431	−0.017	0.044	1.769
Pinus strobus	−0.678	−0.004	−2.150	−0.015	0.023	−0.932
Quercus rubra	−0.449	0.024	−0.143	−0.001	−0.001	0.089
Quercus velutina	−0.305	0.018	0.012	0.000	0.000	0.444
Tsuga canadensis	0.648	−0.021	0.582	0.004	−0.034	−3.086

Table 2
Comparison of allometric models with random effects of plot and species both included (A), only plot excluded (B) and plot and species both excluded (C) from model predictions.

	A. Varied plot effect			B. Mean plot effect			C. Mean species effect		
	ρr^2	RMSE	CV(RMSE)	ρr^2	RMSE	CV(RMSE)	ρr^2	RMSE	CV(RMSE)
Crown radius	0.618	1	31.80%	0.434	1.22	38.80%	0.204	1.44	45.98%
Crown depth	0.471	2.93	29.60%	0.35	3.24	32.80%	0.133	3.74	37.84%
Total height	–	–	–	0.701	2.96	13.80%	0.601	3.42	15.96%

Table 4
Comparisons of mean heights for lidar and synthetic canopy height models for uncorrected and error and bias corrected allometric canopy height models and results of correlation analysis within and across species.

	Uncorrected	Bias-corrected	Imputed CR error	Imputed Ht error	Imputed CR + Ht errors
	a. Canopy height models summary data				
Number of trees	26,858	26,879	21,907	27,376	22,540
Mean pixels per tree	11.34	11.34	14.78	11.13	14.35
Lidar Mean*(Max)* Height	18.99*(20.17)*	18.99*(20.17)*	19.31*(20.69)*	19.06*(20.25)*	19.35*(20.75)*
Allometric Mean*(Max)* Height	12.91*(13.72)*	13.09*(13.90)*	14.16*(14.98)*	13.19*(14.01)*	14.23*(15.09)*
Difference Mean*(Max)*	6.08*(6.45)*	5.9*(6.27)*	5.15*(5.71)*	5.87*(6.24)*	5.12*(5.66)*
	b. Tree height correlations - Pearson's r				
All individuals	0.4917	0.4922	0.4941	0.4736	0.4764
All sampled *(% of crown area)*	0.3568 *(84.6)*	0.3568 *(84.6)*	0.3520 *(88.9)*	0.3424 *(84.6)*	0.3370 *(88.9)*
Tsuga canadensis	0.1711 *(20.1)*	0.1710 *(20.1)*	0.1774 *(19.8)*	0.1790 *(21.2)*	0.1881 *(21.2)*
Acer rubrum	0.3910 *(18.4)*	0.3915 *(18.4)*	0.3742 *(20.6)*	0.3713 *(18.9)*	0.3545 *(21.3)*
Quercus rubra	0.5832 *(27.1)*	0.5831 *(27.1)*	0.4965 *(28.0)*	0.4746 *(26.0)*	0.3805 *(26.7)*
Betula alleghaniensis	0.1008 *(2.6)*	0.1008 *(2.6)*	0.0819 *(2.6)*	0.1014 *(2.8)*	0.0987 *(2.8)*
Pinus strobus	0.5994 *(6.7)*	0.6044 *(6.7)*	0.5811 *(7.4)*	0.4949 *(6.1)*	0.4819 *(6.6)*
Fagus grandifolia	-0.0715 *(1.2)*	-0.0726 *(1.2)*	-0.1344 *(1.4)*	-0.0547 *(1.2)*	-0.0702 *(1.4)*
Betula lenta	0.1038 *(2.2)*	0.0996 *(2.2)*	0.0872 *(2.1)*	0.0996 *(2.3)*	0.0519 *(2.3)*
Pinus resinosa	0.4620 *(2.5)*	0.4613 *(2.5)*	0.2987 *(2.8)*	0.1904 *(2.4)*	0.1230 *(2.6)*
Kalmia latifolia	0.0876 *(0.2)*	0.0894 *(0.2)*	0.1015 *(0.2)*	0.0673 *(0.2)*	0.0805 *(0.2)*
Picea abies	-0.0140 *(0.7)*	-0.0156 *(0.7)*	0.0848 *(0.7)*	0.0204 *(0.8)*	0.1004 *(0.7)*
Betula papyrifera	0.5773 *(1.3)*	0.5765 *(1.3)*	0.5350 *(1.5)*	0.5077 *(1.2)*	0.4657 *(1.4)*
Quercus velutina	0.7310 *(1.3)*	0.7306 *(1.3)*	0.6607 *(1.4)*	0.5238 *(1.2)*	0.4069 *(1.2)*
Fraxinus americana	0.4318 *(0.3)*	0.4315 *(0.3)*	0.4886 *(0.3)*	0.4523 *(0.3)*	0.5354 *(0.3)*
Picea rubens	0.1812 *(0.1)*	0.1746 *(0.1)*	0.0468 *(0.1)*	0.2055 *(0.1)*	0.1077 *(0.1)*

further by imputing crown radius and height errors, particularly crown radius. However, for all species, canopy heights estimated from the lidar CHM were higher than those from the synthetic CHM (Tables 4–6), with less dramatic, but still significant differences among dominant canopy species such as *Quercus rubra*, *Pinus strobus*, *Pinus resinosa*, *Acer rubrum*, and *Betula papyrifera*, among others. The most notable discrepancies occurred for understory species such as *Kalmia latifolia, Vaccinium corymbosum, Hamamelis virginiana, Castanea dentata,*

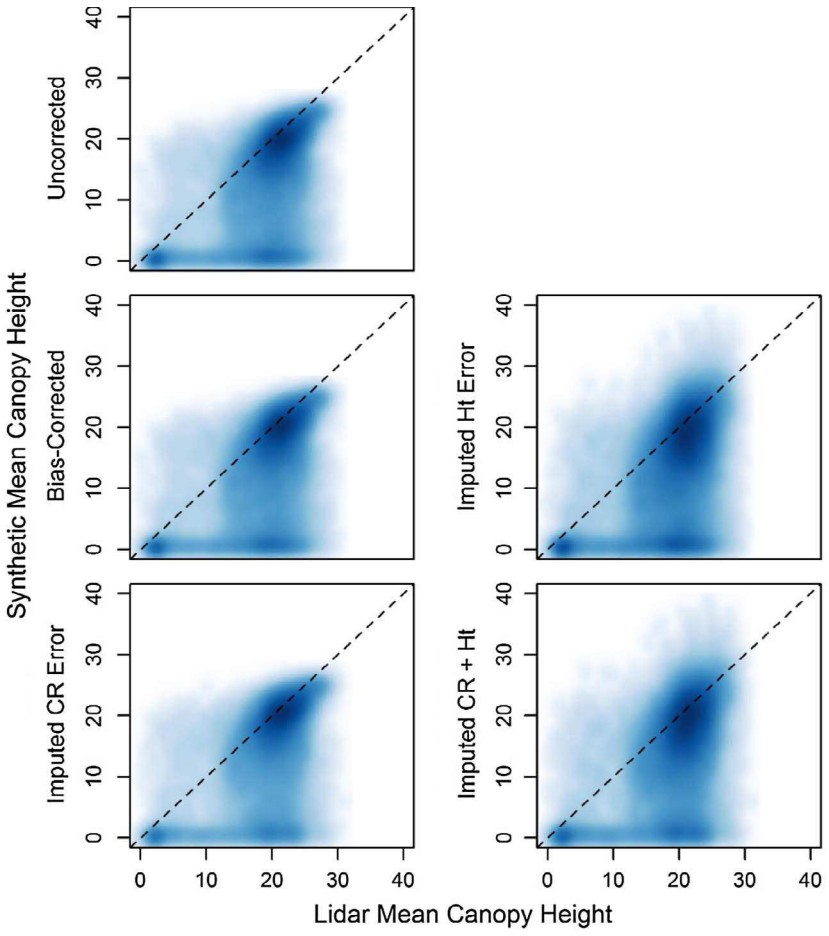

Fig. 3. Color density scatter plots of mean canopy height from lidar-derived and synthetic CHM canopy height models, showing general agreement at the tree level.

Table 5
Comparison of individual-tree mean canopy heights by species as estimated by lidar and synthetic canopy height models using paired *t*-tests.

		Uncorrected		Bias-Corrected		Imputed CR		Imputed height		Imputed CR + height	
Species	Mean N (stems)	Lidar	Synthetic	Lidar	Synthetic	Lidar	Synthetic	Lidar	Synthetic	Lidar	Synthetic
Tsuga canadensis[a]	6761	19.58	11.68	19.58	11.85	19.85	12.92	19.61	11.94	19.86	13.02
Acer rubrum[a]	6013	18.72	14.53	18.72	14.74	18.78	15.36	18.82	14.89	18.89	15.51
Quercus rubra[a]	3381	21.66	19.68	21.66	19.96	21.86	20.49	21.66	19.94	21.85	20.55
Betula alleghaniensis[a]	1359	18.03	9.14	18.03	9.27	18.26	9.81	18.06	9.33	18.28	9.95
Pinus strobus[a]	1217	21.13	20.06	21.12	20.32	21.34	20.54	21.19	20.38	21.41	20.57
Ilex verticillata	781	7.06	0.29	7.05	0.30	7.01	0.27	7.17	0.30	6.86	0.26
Fagus grandifolia[a]	734	20.63	7.17	20.63	7.29	20.88	8.08	20.67	7.45	20.92	8.16
Betula lenta[a]	709	19.81	13.01	19.81	13.18	19.94	14.26	19.94	13.28	20.02	14.30
Pinus resinosa[a]	730	25.62	23.39	25.62	23.72	25.69	23.99	25.68	23.35	25.76	23.79
Kalmia latifolia[a]	392	18.08	1.94	18.07	1.97	18.25	2.07	18.12	1.95	18.28	2.05
Picea abies[a]	426	23.11	14.62	23.11	14.81	23.12	15.22	23.15	15.12	23.17	15.48
Vaccinium corymbosum	416	8.53	0.57	8.54	0.58	8.51	0.54	8.37	0.58	8.59	0.55
Betula papyrifera[a]	408	18.01	15.64	18.00	15.87	18.35	16.82	18.05	15.58	18.37	16.58
Hamamelis virginiana	354	19.67	2.30	19.66	2.35	19.78	2.02	19.70	2.34	19.91	2.09
Quercus velutina[a]	190	21.43	19.43	21.43	19.81	21.83	20.61	21.47	19.33	*21.78*	*20.23*
Alnus incana	166	4.75	0.87	4.74	0.88	4.82	0.75	4.69	0.82	4.94	0.67
Prunus serotina	135	20.64	14.27	20.66	14.63	21.24	15.39	20.68	14.12	21.24	15.14
Castanea dentata	111	20.49	3.03	20.49	3.10	21.46	3.77	20.47	3.04	21.38	3.41
Fraxinus americana[a]	87	19.36	14.68	19.36	14.89	19.34	16.26	19.35	15.28	*19.74*	*16.84*
Lyonia ligustrina	91	5.92	0.17	5.99	0.17	7.12	0.13	6.12	0.18	6.53	0.12
Nyssa sylvatica	87	14.89	12.41	*14.88*	*12.66*	**15.18**	**14.17**	*14.99*	*12.66*	**14.98**	**14.08**
Toxicodendron vernix	76	5.85	0.58	5.86	0.59	5.75	0.53	5.76	0.58	5.74	0.52
Ilex laevigata	77	9.99	0.90	9.98	0.92	10.75	0.87	9.97	0.89	10.80	0.76
Betula populifolia	64	14.41	10.47	14.41	10.68	14.76	10.80	14.33	10.31	14.18	9.53
Acer pennsylvanicum	53	19.42	5.17	19.55	5.29	19.93	6.00	19.67	4.75	20.31	6.24
Viburnum nudum	48	17.49	0.27	17.43	0.27	17.59	0.26	17.44	0.29	16.73	0.24
Picea rubens[a]	46	**19.29**	**18.42**	**19.36**	**18.72**	**19.05**	**18.21**	**19.52**	**19.68**	**19.52**	**19.52**
Amelancheir laevis	33	12.28	2.82	12.28	2.88	14.55	2.42	11.62	2.53	13.55	2.45
Quercus alba	29	***19.78***	***17.87***	**19.77**	**18.21**	**19.46**	**18.74**	**19.99**	**18.05**	**19.85**	**18.49**
Crataegus spp	16	22.61	1.37	22.61	1.40	21.86	2.81	22.62	1.34	22.06	2.65
Sorbus americana	13	14.91	7.57	15.19	8.20	16.82	6.30	15.07	9.01	16.48	7.09
Viburnum dentatum	9	8.65	0.17	8.78	0.17	*8.54*	*0.18*	*8.53*	*0.25*	*7.38*	*0.20*
Quercus spp	11	**19.02**	**15.27**	**19.02**	**15.61**	**19.47**	**17.56**	***18.81***	***13.71***	**19.67**	**15.91**
Unknown	12	20.75	9.34	20.70	9.55	*20.72*	*10.66*	21.12	10.31	*20.78*	*10.94*
Ostrya virginiana	8	18.69	3.75	18.69	3.83	*19.72*	*2.23*	18.63	4.20	*19.72*	*2.61*
Picea spp	10	***18.24***	***12.33***	***18.24***	***12.59***	**18.62**	**16.35**	*19.29*	*13.07*	**19.67**	**16.50**
Fraxinus nigra	8	16.40	8.26	*16.40*	*8.44*	***16.39***	***8.91***	*18.14*	*8.89*	***16.28***	***8.55***
Prunus pensylvanica	6	14.88	6.87	14.88	7.02	*14.87*	*6.11*	*14.81*	*7.30*	***14.57***	***5.83***
Betula spp	5	**15.10**	**9.80**	**15.10**	**10.01**	**17.13**	**8.20**	**15.11**	**10.57**	**17.13**	**7.31**
Picea mariana	7	**19.74**	**19.06**	**19.74**	**19.44**	**18.79**	**19.23**	**19.22**	**19.08**	**18.29**	**18.91**
Rhododendron prinophyllum	6	*20.89*	*0.20*	20.30	0.18	18.87	0.14	*20.89*	*0.22*	18.90	0.17
Viburnum lantanoides	4	20.97	0.04	20.97	0.04	**19.58**	**0.01**	20.97	0.05	–	–
Aronia melanocarpa	3	2.62	0.01	2.62	0.01	**7.17**	**0.03**	2.62	0.01	**7.17**	**0.02**
Lindera benzoin	3	*20.95*	*0.26*	*20.95*	*0.27*	***21.96***	***0.34***	*20.95*	*0.13*	*21.76*	*0.17*
Pinus spp	2	***24.57***	***10.20***	**24.57**	**10.41**	22.95	7.93	***24.57***	***10.08***	22.95	7.69
Acer saccharum	1	24.10	4.34	24.10	4.44	–	–	24.10	4.49	–	–
Juniperus communis	1	2.45	0.22	2.45	0.22	1.77	0.17	2.45	0.17	1.53	0.15
Populus grandidentata	1	15.50	15.05	15.50	15.35	14.90	15.79	15.43	16.54	14.84	16.88
Populus tremuloides	1	15.04	12.06	15.04	12.31	14.49	12.34	15.04	12.66	14.49	12.69
Rhamnus frangula	1	3.12	0.00	3.12	0.00	–	–	3.12	0.00	–	–
Sambucus racemosa	1	–	–	–	–	17.69	0.00	–	–	–	–
Viburnum acerfolium	2	–	–	–	–	–	–	–	–	**19.58**	**0.02**

$p < .001$, $p < .01$, $\mathbf{p < .05}$, not significant.
[a] Species sampled for crown measurements.

Acer pennsylvanicum, and *Viburnum nudum*. These species do not attain heights exceeding a few meters at most in this forest (or in any known habitat). Though the synthetic CHM mean canopy heights indicated lower canopy heights, the lidar CHM indicated canopy heights reaching that of the dominant trees for this site. Thus, the differences between the CHM mean canopy heights for these species must be attributed to species misclassification at the pixel level resulting from dominant canopy trees overtopping understory trees, rather than error in the allometric predictions.

3.3. Canopy height models and power spectra analysis

The resulting FFT 1-d power spectra showed general whole-image scale agreement between all synthetic CHMs and the lidar CHM at longer spatial wavelengths (Figs. 4 and 5). However, at scales smaller than the whole image, we observed differences between all synthetic CHMs and the lidar CHM. Using *t*-tests, there is no significant difference between the lidar CHM and synthetic CHM at spatial wavelengths longer than approximately 64 m, or the length of about 3–4 crown widths of canopy trees. At shorter wavelengths, we found that synthetic CHMs had significantly higher power ($p < .05$) than the lidar CHM. Relative to the other synthetic CHMs, those that accounted for errors in crown radius by error imputation had lower power at short spatial wavelengths and were in closer agreement with the lidar CHM, though they were still significantly different.

Table 6
Comparison of individual-tree maximum canopy heights by species as estimated by lidar and synthetic canopy height models using paired *t*-tests.

		Uncorrected		Bias-corrected		Imputed CR		Imputed height		Imputed CR + height	
Species	Mean N (stems)	Lidar	Synthetic	Lidar	Synthetic	Lidar	Synthetic	Lidar	Synthetic	Lidar	Synthetic
Tsuga canadensis[a]	6761	20.86	12.47	20.85	12.64	21.29	13.76	20.91	12.77	21.32	13.90
Acer rubrum[a]	6013	20.03	15.49	20.03	15.70	20.23	16.27	20.13	15.85	20.36	16.47
Quercus rubra[a]	3381	22.88	20.89	22.88	21.16	23.12	21.69	22.88	21.16	23.14	21.80
Betula alleghaniensis[a]	1359	19.09	9.80	19.09	9.93	19.47	10.47	19.15	9.99	19.52	10.63
Pinus strobus[a]	1217	23.11	21.09	23.09	21.36	23.41	21.55	23.10	21.39	23.42	21.58
Ilex verticillata	781	7.29	0.34	7.29	0.34	8.00	0.33	7.42	0.35	7.86	0.34
Fagus grandifolia[a]	734	21.41	7.64	21.41	7.76	21.88	8.58	21.46	7.93	21.91	8.65
Betula lenta[a]	709	20.93	13.74	20.93	13.91	21.24	15.04	21.09	14.05	21.37	15.13
Pinus resinosa[a]	730	27.37	24.30	27.37	24.62	27.38	24.84	27.40	24.27	27.44	24.67
Kalmia latifolia[a]	392	18.46	2.07	18.46	2.10	19.10	2.25	18.51	2.07	19.14	2.23
Picea abies[a]	426	23.96	15.18	23.96	15.38	24.02	15.77	24.04	15.72	24.03	16.04
Vaccinium corymbosum	416	9.01	0.67	9.03	0.69	9.95	0.68	8.88	0.70	10.03	0.69
Betula papyrifera[a]	408	19.31	16.59	19.31	16.81	19.68	17.70	19.31	16.52	19.67	17.49
Hamamelis virginiana	354	20.27	2.56	20.26	2.62	20.80	2.28	20.31	2.61	20.93	2.35
Quercus velutina[a]	190	22.64	20.69	22.65	21.09	*23.12*	*21.88*	22.61	20.60	*22.99*	*21.51*
Alnus incana	166	5.09	1.01	5.08	1.02	6.22	0.91	5.04	0.96	6.15	0.81
Prunus serotina	135	21.57	15.01	21.59	15.36	22.46	16.14	21.66	14.86	22.45	15.92
Castanea dentata	111	20.88	3.23	20.88	3.30	21.99	4.07	20.86	3.24	21.90	3.69
Fraxinus americana[a]	87	20.27	15.43	20.27	15.64	20.59	17.12	20.31	16.02	*20.99*	*17.74*
Lyonia ligustrina	91	6.06	0.20	6.15	0.20	7.85	0.18	6.25	0.21	7.38	0.17
Nyssa sylvatica	87	15.81	13.08	*15.81*	*13.33*	*16.72*	*14.83*	*15.85*	*13.32*	***16.54***	***14.74***
Toxicodendron vernix	76	6.24	0.66	6.24	0.67	6.87	0.64	6.12	0.68	6.73	0.62
Ilex laevigata	77	10.56	1.04	10.56	1.06	12.32	1.01	10.46	1.02	12.42	0.92
Betula populifolia	64	15.35	11.07	15.35	11.29	16.36	11.35	15.16	10.89	15.71	10.12
Acer pennsylvanicum	53	20.24	5.53	20.36	5.64	21.31	6.36	20.41	5.09	21.75	6.62
Viburnum nudum	48	17.66	0.31	17.60	0.32	18.25	0.31	17.55	0.33	17.34	0.28
Picea rubens[a]	46	**20.67**	**19.45**	**20.76**	**19.77**	**20.18**	**19.00**	**20.77**	**20.65**	**20.66**	**20.38**
Amelancheir laevis	33	12.52	2.93	12.52	2.99	15.28	2.62	11.81	2.62	14.24	2.62
Quercus alba	29	***21.29***	***18.83***	***21.29***	***19.18***	**21.28**	**19.64**	***21.52***	***19.09***	*21.63*	*19.48*
Crataegus spp	16	22.86	1.54	22.86	1.58	22.52	3.04	22.85	1.50	22.46	2.86
Sorbus americana	13	16.14	8.02	16.33	8.62	17.82	6.58	16.50	9.53	17.69	7.46
Viburnum dentatum	9	8.80	0.18	8.92	0.17	*9.10*	*0.30*	*8.76*	*0.26*	*8.03*	*0.32*
Quercus spp	11	**19.56**	**16.22**	**19.56**	**16.55**	**20.30**	**18.50**	***19.37***	***14.55***	**20.32**	**16.70**
Unknown	12	22.24	9.99	22.24	10.19	22.06	11.23	22.58	11.02	*22.18*	*11.63*
Ostrya virginiana	8	18.89	3.95	18.89	4.03	20.35	2.58	18.89	4.47	20.35	3.02
Picea spp	10	***18.93***	***12.87***	***18.93***	***13.12***	**19.73**	**17.11**	*19.81*	*13.51*	**20.97**	**17.47**
Fraxinus nigra	8	*16.74*	*8.58*	*16.74*	*8.75*	***17.60***	***9.52***	*18.64*	*9.28*	*17.73*	*9.10*
Prunus pensylvanica	6	15.36	7.18	15.36	7.33	*15.56*	*6.43*	*15.40*	*7.77*	***15.27***	***6.22***
Betula spp	5	***17.38***	***10.44***	**17.38**	**10.63**	**19.55**	**8.47**	**17.40**	**11.22**	**19.55**	**7.58**
Picea mariana	7	**21.84**	**20.12**	**21.84**	**20.50**	**19.71**	**20.01**	**21.45**	**20.08**	**19.52**	**19.75**
Rhododendron prinophyllum	6	*20.89*	*0.20*	20.30	0.18	19.21	0.18	*20.89*	*0.22*	19.11	0.20
Viburnum lantanoides	4	20.97	0.04	20.97	0.04	–	–	20.97	0.05	–	–
Aronia melanocarpa	3	2.62	0.01	2.62	0.01	**7.17**	**0.03**	2.62	0.01	**7.17**	**0.02**
Lindera benzoin	3	*20.95*	*0.26*	*20.95*	*0.27*	***22.31***	***0.55***	*20.95*	*0.13*	*21.91*	*0.23*
Pinus spp	2	***25.19***	***10.61***	**25.19**	**10.82**	23.18	8.35	***25.19***	***10.49***	23.18	8.11
Acer saccharum	1	25.56	4.76	25.56	4.86	–	–	25.56	4.92	–	–
Juniperus communis	1	2.45	0.22	2.45	0.22	7.80	0.32	2.45	0.17	3.12	0.27
Populus grandidentata	1	17.13	16.11	17.13	16.42	17.13	16.45	17.13	17.63	17.13	17.66
Populus tremuloides	1	16.71	13.05	16.71	13.30	15.10	13.20	16.71	13.65	15.10	13.55
Rhamnus frangula	1	3.12	0.00	3.12	0.00	–	–	3.12	0.00	–	–
Sambucus racemosa	1	–	–	–	–	17.69	0.00	–	–	–	–
Viburnum acerfolium	2	–	–	–	–	**19.58**	**0.01**	–	–	**19.58**	**0.02**

p < .001, *p < .01*, ***p < .05***, **not significant**.
[a] Species sampled for crown measurements.

4. Discussion

4.1. Tree allometry and crown plasticity effects

The general relationships between tree height and *DBH* that we observed across species were qualitatively similar to other relationships that have been reported, with stems between 10–15 m tall at around 15–20 cm *DBH*, reaching 20–25 m tall by 50 cm *DBH* (e.g. Ducey, 2012). There was no clear pattern between predictions for angiosperm vs. gymnosperm or deciduous vs. evergreen species (though these are nearly identical in the data, with the only evergreen angiosperm being *Kalmia latifolia*, which is confined to the low understory; gymnosperm species are listed in bold font in Tables 5 and 6). By contrast, Ducey (2012) did identify patterns in height-diameter scaling associated with species evergreenness and wood specific gravity in this region. However, that study employed a much larger regional dataset (over 200,000 individual trees) and also identified a strong local effect on scaling, which was hypothesized to be due to a combination of climate, site quality (i.e. conditions dictating the type, size, and quality of trees in a site), and past competition. The latter two factors almost certainly vary across the Prospect Hill tract and would be expected to obscure interspecific variation in a study with a limited sample size. Height-diameter allometry is not a fixed species attribute, but the outcome of dynamic and plastic allocation between primary and secondary growth (Niklas, 1995; Oliver and Larson, 1996, ch. 3; Purves et al., 2008; Franklin et al., 2012).

In comparison with the relationships for tree height and crown depth, the variability in species-specific relationships between crown

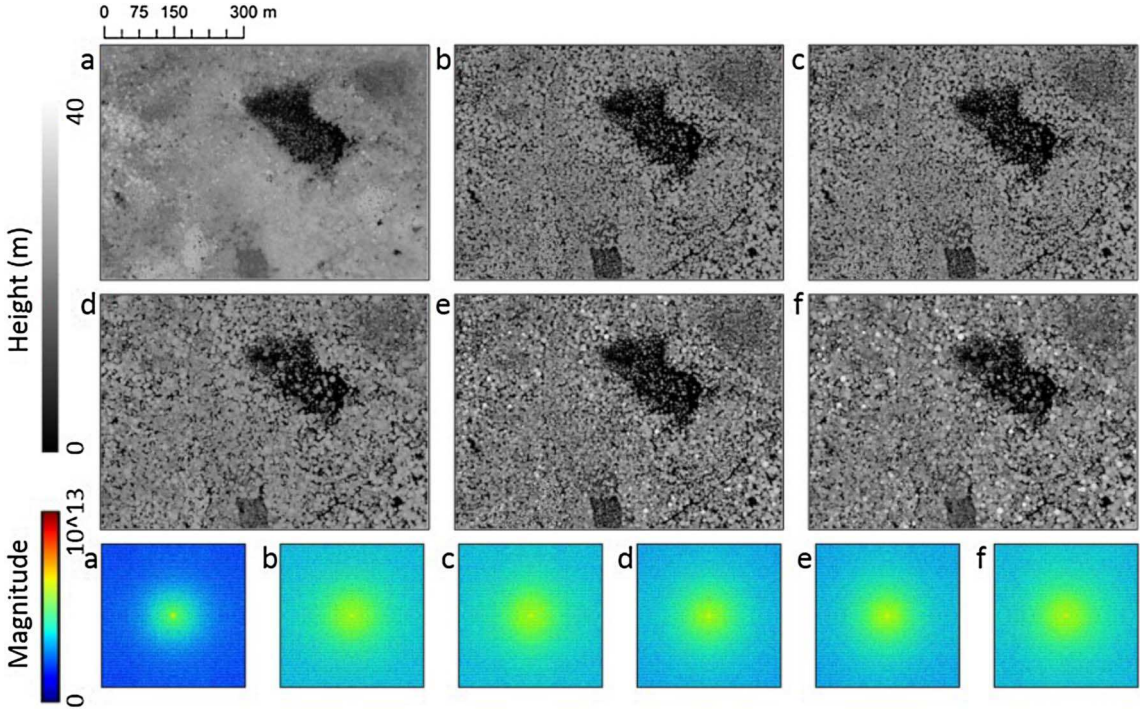

Fig. 4. Canopy height models (top) and their FFTs (bottom) derived from (a) lidar data and (b–e) allometric equations with (b) no error correction, (c) retransformation bias correction, (d) imputed crown radius errors, (e) imputed height errors, (f) imputed crown radius and height errors. FFT results are plotted on a logarithmic color scale.

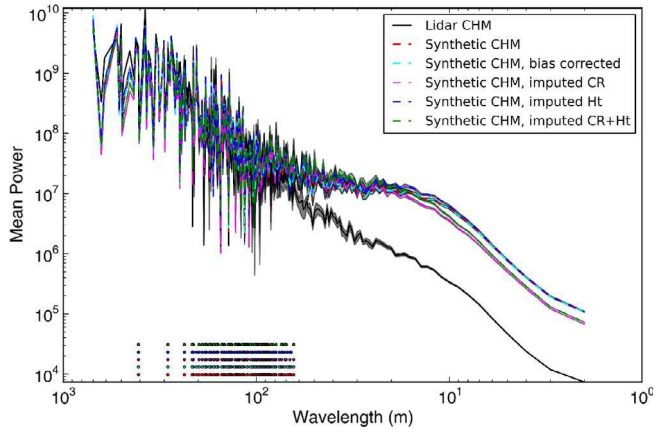

Fig. 5. Power spectra of lidar and synthetic CHMs. Points indicate the spatial wavelengths at which differences between the lidar CHM and the synthetic CHM with the matching color line are not significant.

radius and *DBH* was greater. In general, crown radius slopes were steeper for deciduous angiosperms than needleleaf gymnosperms. To some extent, this effect may be influenced by species-specific carbon allocation strategies that are driven by light availability and competition (Purves et al., 2008, Dybzinski et al., 2015). For example, American beech (*Fagus grandifolia*) is a shade-tolerant deciduous species, and tended to be shorter but with a larger crown radius at a given *DBH* than other species. American beech is among a group of shade tolerant species which typically present with slower vertical growth and substantial plasticity in branching patterns (Canham, 1988). Other shade tolerant deciduous species, including red maple (*Acer rubrum*), red oak (*Quercus rubra*), and yellow birch (*Betula alleghaniensis*) exhibited similar rates of change of crown radius with *DBH*, while lesser shade tolerant and shade intolerant deciduous species, such as black birch (*Betula lenta*) and paper birch (*Betula papyrifera*) presented narrower crowns. Shade tolerance is a key functional trait structuring plant communities (Valladares and Niinemets, 2008). However, an alternative hypothesis would tie the crown radius-DBH relationship to the structural properties of the trees.

Wood specific gravity is a strong proxy for a range of wood properties that would affect branch load-bearing capacity, longevity, and hydraulic transport (Chave et al., 2009), and has been successfully used in models of growing space occupancy and forest stocking in this and similar regions (Ducey and Knapp, 2010; Ducey et al., 2017). Although such models are tied to a more abstract concept of resource space (*sensu* Oliver and Larson, 1996) than to physical space occupancy, their origin is in biomechanical models relating stem strength to canopy mass (Dean and Baldwin, 1996). To further explore these competing hypotheses, we used average shade tolerance rankings for each species from Niinemets and Valladares (2006), which range from 1 for very intolerant species to 5 for very tolerant species, and wood specific gravity values from Miles and Smith (2009), except *Kalmia latifolia* which was taken from USFS FPL (1931). The relationships between the species effects (γ_0 and γ_1) between these two sets of functional traits were evaluated using Spearman's ρ (Fig. 6). The only statistically significant relationship was between γ_1 and wood specific gravity, and was positive consistent with the biomechanical approach of Dean and Baldwin (1996) and its use in mixed-species stand density models (Ducey and Knapp, 2010). This result suggests that specific gravity as a functional trait may be useful as a covariate in refining local crown architecture relationships.

The slope for the *DBH*-crown radius relationship for red pine was much shallower than other species measured in this study, and it lies the farthest (in absolute value) from the central trend of the relationship between the slope and wood specific gravity. The red pine stands at Harvard Forest on Prospect Hill are remnant plantations on which nutrient amendment studies have been conducted (Rainey et al., 1999), and site nutrient status influences allometric relationships in trees (Albaugh et al., 1998, Niinemets and Lukjanova, 2003; Urban et al., 2013). The relationships for red pine that we observed in this study could also be attributed to the spacing, structure and growth of trees in monolayer canopies, which could have influenced competitive dynamics and dictated the extent to which lateral branching would occur for individual trees (e.g. Oliver and Larson, 1996, ch. 3; Pretzsch and Rais, 2016). Departure from typical trends may thus result from a

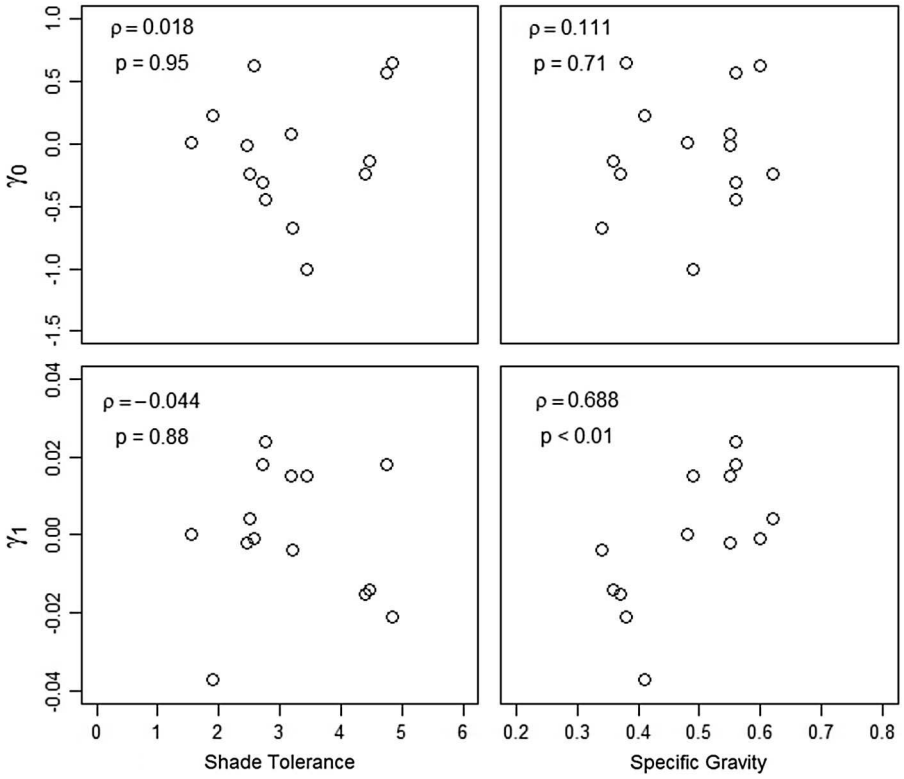

Fig. 6. Scatter plots showing relationships between shade tolerance and specific gravity and species effects from this study.

strong local effect (*sensu* Ducey, 2012) driven by the plantation spacing and subsequent history of these specific plantations.

4.2. Outcomes of bias correction, error imputation, and FFT analysis

Log-transformation (and other nonlinear transformation) is a common practice in developing allometric relationships for biomass and other tree attributes, and it has been long understood that such transformation can result in prediction bias of practical importance if no corrective action is taken (Finney, 1941; Zar, 1968; Baskerville, 1972). It is intuitive that biased predictions could lead to corresponding errors in the development of a fully-synthetic CHM from allometric predictions, or in the assignment of values from a LiDAR-derived CHM back to a given population of trees. However, the development of CHMs and their subsequent segmentation and assignment to individual trees are both nonlinear processes. Where nonlinearity is present, the propagation of variance (or lack thereof) may also exert an important influence, as has been noted in other ecological contexts (e.g. Band et al., 1991). In our study, closed-form correction of allometric bias in tree height (e.g. Baskerville, 1972), imputation of residuals from the tree height model, and imputation of residuals from the crown radius and tree height models together led to progressive increases in synthetic CHM canopy heights, and better matches between those and corresponding heights in a LiDAR-derived CHM (where the sole influence of allometric prediction was in the assignment of individual pixels to mapped trees). However, none of these techniques could fully correct evident errors in tree assignment and in the CHM surface itself, especially at high spatial frequencies.

One challenge for both the synthetic CHMs and the assignment of pixels to trees in the LiDAR CHM is the inflexible description of tree form implicit in our use of the allometric models. Tree crowns were assumed to be centered over the mapped stem location and to be symmetrical. However, many trees lean for a variety of reasons, and leaning trees may have crown centers displaced by several meters from the location of the stem near ground level (Gatziolis et al., 2010). Crown plasticity is another major challenge for modeling forest canopy structure (Purves et al., 2007). Changes in shoot-level architecture and whole-plant resource allocation in response to overhead shade, lateral competition, and physical crown abrasion can all alter the crown form of individual trees (Oliver and Larson, 1996, ch. 3). This results in much more efficient capture of resources and filling of physical space than would occur in the absence of crown plasticity, and the effect is more dramatic in mixed-species forests (such as the one studied here) than in monocultures (Pretzsch, 2014). The rigid application of a “popsicle” tree form, without regard to neighborhood context, leads to trees in our synthetic CHMs that have physically impossible crown overlap in three-dimensional space, while they also fail to exploit space along the predicted crown perimeters where no such overlap exists. As a result, the synthetic CHMs show much greater height variation and canopy roughness at small spatial scales. The elliptical crown form assumption employed may also fail to capture the umbrella-shaped canopy associated with many hardwood trees with decurrent stem form (e.g. Ford, 1985), thus leading to steeper falloff and deeper canyons in the synthetic CHM as compared with the LiDAR-derived CHM. Both sources of error would contribute to mis-assignment of relatively high-elevation pixels to understory trees and shrubs, if the tendency of dominant trees to more fully exploit space at the top of the canopy was underestimated. The improved ability to represent individual tree crowns and their plasticity within a tractable framework remains an important area of work across multiple applications (Purves et al., 2007, 2006). Nonetheless, the close correspondence in power between the synthetic and LiDAR-derived CHMs at spatial wavelengths above ~60 m does suggest a good ability to map and simulate canopy properties at moderate resolution using this approach.

5. Conclusions

Our mixed effects allometric equations for crown geometry and tree height provide some insight into variability in crown structure across species in an eastern deciduous forest. Estimates of height, crown radius, and crown depth, and how they relate to stem diameter were on par with previous studies. However, due to challenges related to inter-

and intra-specific competition, crown plasticity, and the use of an overly simplistic tree form, we observed a general negative bias at the tree level in synthetic CHM canopy heights relative to lidar CHM canopy heights. Our tree level canopy height results were marginally improved by error imputation and bias correction approaches, but these approaches could not overcome the shortcomings in our synthetic CHM derivation. However, using an FFT analysis, we determined that an apparent bias in crown radius estimation could be partially overcome through error imputation, suggesting that allowing for crown plasticity or accounting for leaning stems in synthetic CHM development could make some headway towards improving on this particular application of our allometric models. Allometric model-based derivation of canopy height models could be a useful tool for providing contextual information about forest canopies to researchers using both optical and lidar remote sensing on airborne and satellite platforms. In conjunction with improvements to existing crown delineation algorithms, links between tree crown geometry and *DBH* like the ones presented in this paper could have utility for biomass estimation and species and structural characterization on an individual tree basis with data fusion approaches that use high spatial resolution lidar and hyperspectral data.

Acknowledgements

The authors thank numerous volunteers for field assistance. Many seasons of field technicians assisted in census data set collection. This research was supported by NASA New Investigators in Earth Science (NNX10AQ82G), NASA Terrestrial Ecology (NNX08AL29G), NASA IDS (NNX14AD31G), and NSF Macrosystems (NSF Grant #1638688). This research is a publication of the Harvard Forest LTER Program (NSF DEB 12-37491).

References

Albaugh, T.J., Allen, H.L., Dougherty, P.M., Kress, L.W., King, J.S., 1998. Leaf area and above-and belowground growth responses of loblolly pine to nutrient and water additions. Forest Sci. 44 (2), 317–328.

Andersen, H.E., Reutebuch, S.E., McGaughey, R.J., d'Oliveira, M.V.N., Keller, M., 2014. Monitoring selective logging in western Amazonia with repeat lidar flights. Remote Sens. Environ. 151, 157–165.

Anderson-Teixeira, K.J., et al., 2015. CTFS-ForestGEO: A worldwide network monitoring forests in an era of global change. Global Change Biol. 21, 528–549. http://dx.doi.org/10.1111/gcb.12712.

Asner, G.P., Palace, M., Keller, M., Pereira, R., Silva, J.N.M., Zweede, C., 2002. Estimation canopy structure in an Amazon forest from laser range finder and IKONOS satellite observations. Biotropica 34, 483–492.

Asner, G.P., Mascaro, J., Muller-Landau, H.C., Vieilledent, G., Vaudry, R., Rasamoelina, M., et al., 2012. A universal airborne LiDAR approach for tropical forest carbon mapping. Oecologia 168 (4), 1147–1160.

Band, L.E., Peterson, D.L., Running, S.W., Coughlan, J., Lammers, R., Dungan, J., Nemani, R., 1991. Forest ecosystem processes at the watershed scale: basis for distributed simulation. Ecol. Model. 56, 171–196.

Baskerville, G.L., 1972. Use of logarithmic regression in the estimation of plant biomass. Can. J. For. Res. 2, 49–53.

Bitterlich, W., 1984. The relascope idea: relative measurements in forestry, 1st ed. Commonwealth Agricultural Bureaux, Slough, UK.

Broadbent, E.N., Asner, G.P., Peña-Claros, M., Palace, M., Soriano, M., 2008. Spatial partitioning of biomass and diversity in a lowland Bolivian forest: linking field and remote sensing measurements. For. Ecol. Manage. 255, 2602–2616.

Canham, C., 1988. Growth and canopy architecture of shade-tolerant trees: response to canopy gaps. Ecology 69 (3), 786–795.

Chave, J., Andalo, C., Brown, S., Cairns, M., Chambers, J.C., Eamus, D., et al., 2005. Tree allometry and improved estimation of carbon stocks and balance in tropical forests. Oecologia 145 (1), 87–89.

Chave, J., Coomes, D., Jansen, S., Lewis, S.L., Swenson, N.G., Zanne, A.E., 2009. Towards a worldwide wood economics spectrum. Ecol. Lett. 12, 351–366.

Cook, B.D., Corp, L.W., Nelson, R.F., Middleton, E.M., Morton, D.C., McCorkel, J.T., Masek, J.G., Ranson, K.J., Ly, V., Montesano, P.M., 2013. NASA Goddard's Lidar, Hyperspectral and Thermal (G-LiHT) airborne imager. Remote Sens. 5, 4045–4066. http://dx.doi.org/10.3390/rs5084045.

Czaplewski, R.L., Bruce, D., 1990. Retransformation bias in a stem profile model. Can. J. For. Res. 20 (10), 1623–1630.

Dalponte, M., Coomes, D.A., 2016. Tree-centric mapping of forest carbon density from airborne laser scanning and hyperspectral data. Methods Ecol. Evol. 7, 1236–1245.

Dean, T.J., Baldwin Jr., V.C., 1996. The relationship between Reineke's stand-density index and physical stem mechanics. For. Ecol. Manage. 81, 25–34.

Dubayah, R.O., Sheldon, S.L., Clark, D.B., Hofton, M.A., Blair, J.B., Hurtt, G.C., Chazdon, R.L., 2010. Estimation of tropical forest height and biomass dynamics using lidar remote sensing at La Selva, Costa Rica. J. Geophys. Res. 115. http://dx.doi.org/10.1029/2009JG000933.

Ducey, M.J., 2012. Evergreenness and wood density predict height-diameter scaling in trees of the northeastern United States. For. Ecol. Manage. 279, 21–26.

Ducey, M.J., Knapp, R.A., 2010. A stand density index for complex mixed species forests in the northeastern United States. For. Ecol. Manage. 260, 1613–1622.

Ducey, M.J., Woodall, C.W., Bravo-Oviedo, A., 2017. Climate and species functional traits influence maximum stocking in the Lake States, U.S.A. For. Ecol. Manage. 386, 51–61.

Duncanson, L.I., Cook, B.D., Hurtt, G.C., Dubayah, R.O., 2015. An efficient, multi-layered crown delineation algorithm for mapping individual tree structure across multiple ecosystems. Remote Sens Environ 154, 378–386.

Dybzinski, R., Farrior, C.E., Pacala, S.W., 2015. Increased forest carbon storage with increased atmospheric CO2 despite nitrogen limitation: a game-theoretic allocation model for trees in competition for nitrogen and light. Glob. Change Biol. 21, 1182–1196.

Ellis, P., Griscom, B., Walker, W., Goncalves, F., Cormier, T., 2016. Mapping selective logging impacts in Borneo with GPS and airborne lidar. For. Ecol. Manage. 365, 184–196.

Espírito-Santo, F.D.B., Gloor, M., Keller, M., Malhi, Y., Saatchi, S., Nelson, B., et al., 2014. Size and frequency of natural forest disturbances and Amazon carbon balance. Nat. Commun. 5. http://dx.doi.org/10.1038/ncomms4434.

Fast, A.J., Ducey, M.J., 2011. Height-diameter equations for select New Hampshire tree species. Northern J. Appl. For. 28 (3), 157–160.

Feldpausch, T., Banin, L., Phillips, O.L., Baker, T.R., Lewis, S.L., Quesada, C.A., Affum-Baffoe, K., et al., 2011. Height-diameter allometry of tropical trees. Biogeosciences 8 (5), 1081–1106.

Ferraz, A., Saatchi, S., Mallet, C., Meyer, V., 2016. Lidar detection of individual tree size in tropical forests. Remote Sens. Environ. 183, 318–333.

Finney, D.I., 1941. On the distribution of a variable whose logarithm is normally distributed. J. Roy. Stat. Sci Ser. B 7, 155–161.

Ford, E.D., 1985. Branching, crown structure and the control of timber production. In: Cannell, M.G.R., Jackson, J.E. (Eds.), Attributes of Trees as Crop Plants. Abbotts Ripton, Institute of Terrestrial Ecology, pp. 228–252.

Franklin, O., Jahansson, J., Dewar, R.C., Dieckmann, U., McMurtrie, R.E., Brannstrom, A., Dybzinski, R., 2012. Modeling carbon allocation in trees: a search for principles. Tree Physiol. 32, 648–666.

Frolking, S., Palace, M., Clark, D.B., Chambers, J.Q., Shugart, H.H., Hurtt, G.C., 2009. Forest disturbance and recovery - a general review in the context of space-borne remote sensing of impacts on aboveground biomass and canopy structure. J. Geophys. Res. 114, G00E02. http://dx.doi.org/10.1029/2008JG000911.

Gatziolis, D., Fried, J.S., Monleon, V.S., 2010. Challenges to estimating tree height via LiDAR in closed-canopy forests: A parable from Western Oregon. For. Sci. 56 (2), 139–155.

Goodman, R.C., Phillips, O.L., Baker, T.R., 2014. The importance of crown dimensions to improve tropical tree biomass estimates. Ecol. Appl. 24 (4), 680–698.

Gregoire, T.G., Valentine, H.T., 1995. A sampling strategy to estimate the area and perimeter of irregularly shaped planar regions. For. Sci. 41, 470–476.

Homolová, L., Malenovský, Z., Clevers, J.G.P.W., García-Santos, G., Schaepman, M.E., 2013. Review of optical-based remote sensing for plant trait mapping. Ecol. Complexity 15, 1–16.

Hunter, M.O., Keller, M., Victoria, D., Morton, D.C., 2013. Tree height and tropical forest biomass estimation. Biogeosciences 10, 8385–8399. http://dx.doi.org/10.5194/bg-10-8385-2013.

Jucker, T., Caspersen, J., Chave, J., Antin, C., Barbier, N., Bongers, F., et al., 2017. Allometric equations for integrating remote sensing imagery into forest monitoring programmes. Glob. Change Biol. 23, 177–190.

Kershaw Jr., J.A., Ducey, M.J., Beers, T.W., Husch, B., 2016. Forest Mensuration, fifth ed. Wiley, New York.

Lefsky, M.A., Cohen, W.B., Acker, S.A., Parker, G.G., Spies, T.A., Harding, D., 1999. Lidar remote sensing of the canopy structure and biophysical properties of Douglas-fir western hemlock forests. Remote Sens. Environ. 70 (3), 339–361.

Manuri, S., Andersen, H.E., McGaughey, R.J., Brack, C., 2017. Assessing the influence of return density on estimation of lidar-based aboveground biomass in tropical peat swamp forests of Kalimantan, Indonesia.

Mauya, E.W., Hansen, E.H., Gobakken, T., Ballandsas, O.M., Malimbwi, R.E., Naesset, E., 2015. Effects of field plot size on prediction accuracy of aboveground biomass in airborne laser scanning-assisted inventories in tropical rain forests of Tanzania. Carbon Balance Manage. 10. http://dx.doi.org/10.1186/s13021-015-0021-x.

Meyer, V., Saatchi, S.S., Chave, J., Dalling, J.W., Bohlman, S., Fricker, G.A., Robinson, C., Neumann, M., Hubbell, S., 2013. Detecting tropical forest biomass dynamics from repeated airborne lidar measurements. Biogeosciences 10, 5421–5438.

Miles, P.D., Smith, W.B., 2009. Specific gravity and other properties of wood and bark for 156 tree species found in North America. Newtown Square, PA: USDA For. Serv. Res. Note NRS-38.

Niinemets, U., Lukjanova, A., 2003. Needle longevity, shoot growth and branching frequency in relation to site fertility and within-canopy light conditions in Pinus sylvestric. Ann. For. Sci. 60, 195–208.

Niinemets, Ü., Valladares, F., 2006. Tolerance to shade, drought, and waterlogging of temperate northern hemisphere trees and shrubs. Ecol. Monogr. 76, 521–547.

Niklas, K.J., 1995. Size-dependent allometry of tree height, diameter and trunk-taper. Ann. Bot. 75 (3), 217–227.

Ni-Meister, W., Lee, S., Strahler, A.H., Woodcock, C.E., Schaaf, C., Yao, T., Ranson, K.J., Sun, G., Blair, J.B., 2010. Assessing general relationships between aboveground

biomass and vegetation structure parameters for improved carbon estimate from lidar remote sensing. J. Geophys. Res. Biogeosci. 115 (G2).
Oliver, C.D., Larson, B.C., 1996. Forest Stand Dynamics, update ed.,. John Wiley and Sons Inc., New York, NY ISSN: 0471138339.
Orwig, D.A., Foster, D.R., Ellison, A.M., 2015. Harvard Forest CTFS-ForestGEO Mapped Forest Plot since 2014. Harvard Forest Data Archive: HF253. Available online: http://harvardforest.fas.harvard.edu:8080/exist/apps/datasets/showData.html?id=hf253.
Palace, M., Keller, M., Asner, G.P., Hagen, S., Braswell, B., 2008. Amazon forest structure from IKONOS satellite data and the automated characterization of forest canopy properties. Biotropica 40 (20), 141–150.
Palace, M., Sullivan, F.B., Ducey, M.J., Herrick, C., Zanin Shimbo, J., Mota e Silva, J., 2015. Estimating forest structure in a tropical forest using field measurements, a synthetic model and discrete return lidar data. Remote Sens. Environ. 161, 1–11. http://dx.doi.org/10.1016/j.rse.2015.01.020.
Palace, M., Sullivan, F.B., Ducey, M., Herrick, C., 2016. Estimating tropical forest structure using a terrestrial lidar. PLoS One 11 (4), e0154115. http://dx.doi.org/10.1371/journal.pone.0154115.
Pretzsch, H., 2014. Canopy space filling and tree crown morphology in mixed-species stands compared with monocultures. For. Ecol. Manage. 327, 251–264.
Pretzsch, H., Raisl, A., 2016. Wood quality in complex forests versus even-aged monocultures: review and perspectives. Wood Sci. Technol. 50, 845–880.
Purves, D.W., Lichstein, J.W., Pacala, S.W., 2007. Crown plasticity and competition for canopy space: A new spatially implicit model parameterized for 250 North American tree species. PLoS One 2 (9), e870. http://dx.doi.org/10.1371/journal.pone.0000870.
Purves, D.W., Lichstein, J.W., Strigul, N., Pacala, S.W., 2008. Predicting and understanding forest dynamics using a simple tractable model. PNAS 105 (44), 17018–17022.
Rainey, S.M., Nadelhoffer, K.J., Silver, W.L., Downs, M.R., 1999. Effects of chronic nitrogen additions on understory species in a red pine plantation. Ecol. Appl. 9 (3), 949–957.
Saatchi, S., Harris, N.L., Brown, S., Lefsky, M., Mitchard, E., Salas, W., et al., 2011. Benchmark map of forest carbon stocks in tropical regions across three continents. Proc. Natl. Acad. Sci. 108 (24), 9899–9904.
Schumacher, F.X., Hall, F.D.S., 1933. Logarithmic expression of timber-tree volume. J. Agric. Res. 47, 719–734.
Sinclair, S., Pegram, G.G.S., 2005. Empirical mode decomposition in 2-D space and time: a tool for space-time rainfall analysis and nowcasting. Hydrol. Earth Syst. Sci. 9, 127–137.
Spies, T.A., 1998. Forest Structure: A key to the ecosystem. In: Trofymow, J.A., MacKinnon, A., (Eds.), Proceedings of a Workshop on Structure, Process, and Diversity in Successional Forests of Coastal British Columbia, February 17–19, 1998, Victoria, British Columbia. Northwest Science, Vol. 72 (special issue No. 2), pp. 34–39.
Sullivan, F.B., Palace, M.W., Ducey, M.J., 2014. Multivariate statistical analysis of asynchronous lidar data and vegetation models in a neotropical forest. Remote Sens. Environ. 154, 368–377.
Swetnam, T.L., Falk, D.A., 2014. Application of metabolic scaling theory to reduce error in local maxima tree segmentation from aerial LiDAR. For. Ecol. Manage. 323, 158–167.
Treuhaft, R., Gonçalves, F., dos Santos, J.R., Keller, M., Palace, M., Madsen, S.N., Sullivan, F., Graça, P.M.L.A., 2014. Tropical-forest biomass estimation at X-band from the spaceborne TanDEM-X Interferometer. IEEE Geosci. Remote Sens. Lett. http://dx.doi.org/10.1109/LGRS.2014.2334140.
Urban, J., Holusova, K., Mensik, L., Cermak, J., Kantor, P., 2013. Tree allometry of Douglas fir and Norway spruce on a nutrient-poor and a nutrient-rich site. Trees 27, 97–110.
USFS FPL (United States Forest Service, Forest Products Laboratory), 1931. Weights of various woods grown in the United States. Madison, WI: Forest Products Laboratory Technical Note 218. 8 pages.
Valladares, F., Niinemets, U., 2008. Shade tolerance, a key plant feature of complex nature and consequences. Annu. Rev. Ecol. Evol. Syst. 39, 237–257.
van der Walt, S., Colbert, C., Varoquaux, G., 2011. The NumPy array: A structure for efficient numerical computation. Comput. Sci. Eng. 13, 22–30. http://dx.doi.org/10.1109/MCSE.2011.37.
van Leeuwen, M., Nieuwenhuis, M., 2010. Retrieval of forest structural parameters using LiDAR remote sensing. Eur. J. Forest Res. 129, 749–770.
Xie, Y., Sha, Z., Yu, M., 2008. Remote sensing imagery in vegetation mapping: a review. J. Plant Ecol. 1 (1), 9–23.
Yao, T., Yang, X., Zhao, F., Wang, Z., Zhang, Q., Jupp, D., Lovell, J., Culvenor, D., Newnham, G., Ni-Meister, W., et al., 2011. Measuring forest structure biomass in New England forest stands using the Echidna ground-based lidar. Remote Sens. Environ. 115, 2965–2974.
Zar, J.H., 1968. Calculation and miscalculation of the allometric equation as a model in biological data. Bioscience 18, 1118–1120.
Zhao, K., Popescu, S., Nelson, R., 2009. Lidar remote sensing of forest biomass: A scale-invariant estimation approach using airborne lasers. Remote Sens. Environ. 113 (1), 182–196.